DOI: 10.1002/ejic.200901170

Surface Layer-by-Layer Chemical Deposition Reaction for Nanosized Thin-Film Formation of Metal Complexes of 2-Mercaptonicotinic Acid

Sawsan M. S. Haggag*[a]

Keywords: Layer-by-layer deposition / Thin films / Nanostructures / Thermochemistry / Electron microscopy

2-Mercaptonicotinic acid [H_2mna] reacted with Mn^{II}, Co^{II}, Ni^{II}, Cu^{II}, and Zn^{II} by using a layer-by-layer chemical deposition technique; thin-film nanosized metal–[Hmna]$_2$ complexes were formed. The metal complexes were synthesized by the alternative dipping of a glass substrate into the metal ion solution followed by the ligand solution. A molar stoichiometric ratio of 1:2 was characterized for all newly synthesized nanosized Mn^{II}-, Co^{II}-, Ni^{II}-, Cu^{II}-, and Zn^{II}–2-mercaptonicotinate complexes, as confirmed from analysis of the metal. Electron impact mass spectrometry (EIMS) of the collected particles from the thin-film deposited Mn^{II}[Hmna]$_2$ complex (as a selected example) indicates molecular ion peaks at *m*/*z* values of 155 and 363 amu for [H_2mna] and Mn^{II}[Hmna]$_2$, respectively. The deposited thin films of the nanosized metal complexes were subjected to analysis and imaging by scanning electron microscopy (SEM) and were identified to give a range of detected particle sizes ≥20–130 nm. The five metal–[Hmna]$_2$ complexes were characterized by FTIR spectroscopy, and the ligand was found to bind to the metal through the carboxylic oxygen atom and the mercapto sulfur atom. The UV/Vis spectra of the deposited thin film materials and of the ethanol solutions of the complexes were recorded to identify the possibility of d–d transitions in all newly synthesized metal–[Hmna]$_2$ complexes. Thermal gravimetric analysis (TGA and DTG) was also used to identify the possible thermal degradation processes and to calculate some thermodynamic parameters.

Introduction

Layer-by-layer (LBL) deposition has been identified and proven to be an efficient procedure for the synthesis and construction of multilayered nanostructures and nanomaterials.[1–7] The LBL technique is a simple method based on successive and alternating immersion of charged or uncharged substrate into oppositely charged or neutral electrolytes solutions for thin-film formation. The formation of various materials such as polymers, lipids, proteins, nanoparticles, and optically and electrically active materials through direct assembly on various substrates were reported.[8–11]

LBL chemical deposition was recently used as a simple, direct, and efficient method for thin-film assembly of nanosized metal–8-hydroxyquinolate complexes.[12] The controlling factors affecting thin-film formation of the cobalt(II)–8-hydroxyquinolate complex by LBL chemical deposition were studied, explored, and optimized.[13]

Several other reports also focused on LBL deposition for the synthesis of thin films with various potential applications. Polydiacetylene (PDA) supramolecules were prepared by UV irradiation of molecularly assembled diacetylene monomers. These materials were extensively investigated and evaluated as chemosensors and photonic materials.[14,15] Alternative deposition of oppositely charged linear polymers was also reported for the development of PDA-based chemosensors in layered PDA systems.[16] Zirconium oxide films were produced by sequential LBL adsorption of diluted zirconium alkoxide solutions onto a silicon wafer. The parameters controlling the formation of dense, high-dielectric–constant thin films such as the nature of the films and the conditions required to grow single layers in each deposition step were discussed and reported.[17,18] The fabrication of stable multilayer films was achieved through UV irradiation of LBL self-assembled multilayer films. The driving force for the construction, the thickness and hardness, and the morphological structural changes of the multilayer films were investigated.[19] A new type of polyphenol microcapsules of naturally occurring polyphenol(–)-epigallocatechingallate (EGCG) and gelatin, type A, was also obtained by using the LBL assembly method.[20] Electrostatic LBL deposition and electrochemical characterization of the thin films composed of MnO_2 nanoparticles have been reported.[21] The electrochemical characterization of the LBL deposited thin film with and without the addition of a lithium salt indicated a higher electrochemical response of the nanostructured electrode in the lithium-containing electrolyte.[22] The successive ionic layer adsorption and reaction (SILAR) method of formation of metal chalcogenide thin films were previously reported.[23]

[a] Faculty of Science, Chemistry Department, Alexandria University,
P. O. Box 426, Alexandria 21321, Egypt
E-mail: smsh2006@hotmail.com

2-Mercaptonicotinic acid is characterized by the presence of sulfur, nitrogen, and oxygen donor atoms. The three functional moieties, the mercapto group, the pyridyl ring nitrogen atom, and the carboxylic group, lead to three potential binding sites. Therefore, 2-mercaptonicotinic acid is considered to be an excellent reagent for utilization in various analytical, inorganic, and physical studies and applications. 2-Mercaptonicotinic acid was previously loaded by physical adsorption onto the surface of three alumina phases for selective chelation, separation, extraction, and pre-concentration of lead(II) and copper(II) from water matrices.[24] The kinetics for and mechanism of 2-mercaptonicotinic acid oxidation by potassium ferrate over the pH range 6.7–10.8 was studied and reported.[25] Reactions of silver(I) tetrafluoroborate with 2-mercaptonicotinic acid and bis(diphenylphosphanyl)methane (dppm) was studied and found to afford $[Ag_2(mnic:O,S)(dppm)_2]_2$.[26] The thermal properties of lanthanide complexes[27] and first-row transition-metal complexes (in static air)[28] with 2-mercaptonicotinic acid were evaluated and reported. The antimicrobial activity of mercury(II) complexes of 2-mercaptonicotinic acid derivatives were evaluated.[29] Pd^{II} and Pt^{II} complexes of 2-mercaptonicotinic acid with the formula [M(mercaptonicotinic acid)Cl] were also synthesized and characterized.[30] The interaction of polyfunctional 2-mercaptonicotinic acid with the ruthenium(III)–EDTA complex[31] and the synthesis, crystal structures, and coordination modes of Pd^{II}, Pt^{II}, Re^{III}, and Mo^{VI} complexes of 2-mercaptonicotinic acid were also studied.[32]

Research on and synthetic approaches toward thin-film growth and control of discrete nanometal complexes are not well developed. In addition, the growth of thin films of nanometal complexes represents a challenging research area owing to the specific aimed properties that can be incorporated into these materials. Therefore, the objective of this work is directed and devoted toward developing a new synthetic route and technique for the formation of nanosized thin films of some metal complexes. This trend is based on the reaction of 2-mercaptonicotinic acid (H_2mna) with Mn^{II}, Co^{II}, Ni^{II}, Cu^{II}, and Zn^{II} by using a simple and rapid LBL chemical deposition technique. The evaluation and optimization of important, controlling factors in this process have also been addressed in this report. The structure of the metal–2-mercaptonicotinate complexes deposited onto thin films was characterized and confirmed (Scheme 1). Scanning electron microscopy (SEM), electron impact mass spectrometry (EIMS), UV/Vis spectroscopy, Fourier transform-infrared spectroscopy (FTIR), and thermal analysis technique (TGA and DTG) were used for such structural confirmation.

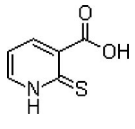

Scheme 1. 2-Mercaptonicotinic acid.

Results and Discussion

Factors Optimization

Thin-film formation of nanomaterials by surface LBL chemical deposition was recently implemented for the synthesis of various important compounds. This process is mainly initiated by the direct deposition of either ionic or molecular species already dissolved in a solution on the surface of a solid support as the first deposited component. The reaction then proceeds by deposition of the second interacting species from its solution onto the same solid support. These two steps of the deposition process represent the formation of the first layer of the aimed compounds. Formation of the multilayer thin film is then completed upon repetition of the LBL deposition steps, to produce the required thickness and homogeneity of the thin film. It has been previously reported that thin-film formation of nanomaterials by using the LBL technique is generally controlled and influenced by several important factors. These include the number of reaction cycles, reaction time, pH value, amongst others.[13] Table 1 represents the studied and optimized factors for thin-film formation of nanosized Mn^{II}- and Cu^{II}–2-mercaptonicotinate complexes.

Table 1. Studied and optimized factors for thin-film formation.

Metal ion	Factors	Specifications
Mn^{II}, Cu^{II}	Dipping times	5, 10, 20, 30, 40 s
	Dipping cycles	2, 5, 10, 15, 20, 25, 30, 35, 40 cycles
	pH	4, 5, 6, 7

Figure 1 a–c shows the effect of various controlling factors on thin-film growth of the nanosized $M[Hmna]_2$ complexes. The effect of the reaction dipping time on the mass loaded on thin films of $Mn[Hmna]_2$ and $Cu[Hmna]_2$ is shown in Figure 1a. It is clear that the mass of $Cu[Hmna]_2$ deposited is higher than that for $Mn[Hmna]_2$ irrespective of the time. In addition, a gradual increase in the deposited thin film is also evident with increasing dipping time. A fast chemical reaction for both Cu^{II} and Mn^{II} with 2-mercaptonicotinic acid could be observed. Uniform and homogeneous thin films of $Cu[Hmna]_2$ and $Mn[Hmna]_2$ were formed after only 6 and 15 dipping cycles, respectively, by using a time period of 10–40 seconds. Figure 1b shows the effect of the number of dipping cycles on the thin-film formation of $Mn[Hmna]_2$ and $Cu[Hmna]_2$ at 20 and 10 s, respectively. In the same manner, the deposited mass of the nanosized $Cu[Hmna]_2$ complex is higher than that of $Mn[Hmna]_2$ irrespective of the number of dipping cycles. The time for the reaction between Cu^{II} and 2-mercaptonicotinic acid is lower than that for Mn^{II}; the reaction with Cu^{II} proceeds at a faster rate. The effect of pH on thin-film formation of the nanosized $M[Hmna]_2$ complexes by LBL deposition was also studied. Four pH values were selected, 4, 5, 6, and 7. Figure 1c shows the results of this study for $Mn[Hmna]_2$ and $Cu[Hmna]_2$ with a dipping time of 10 s. An increase

in the deposited mass of $Mn[Hmna]_2$ and $Cu[Hmna]_2$ was observed with a gradual increase in the pH of the metal ion solution from pH 4 to 6. The optimum pH value for thin-film formation for these two metal complexes was found to be 6.

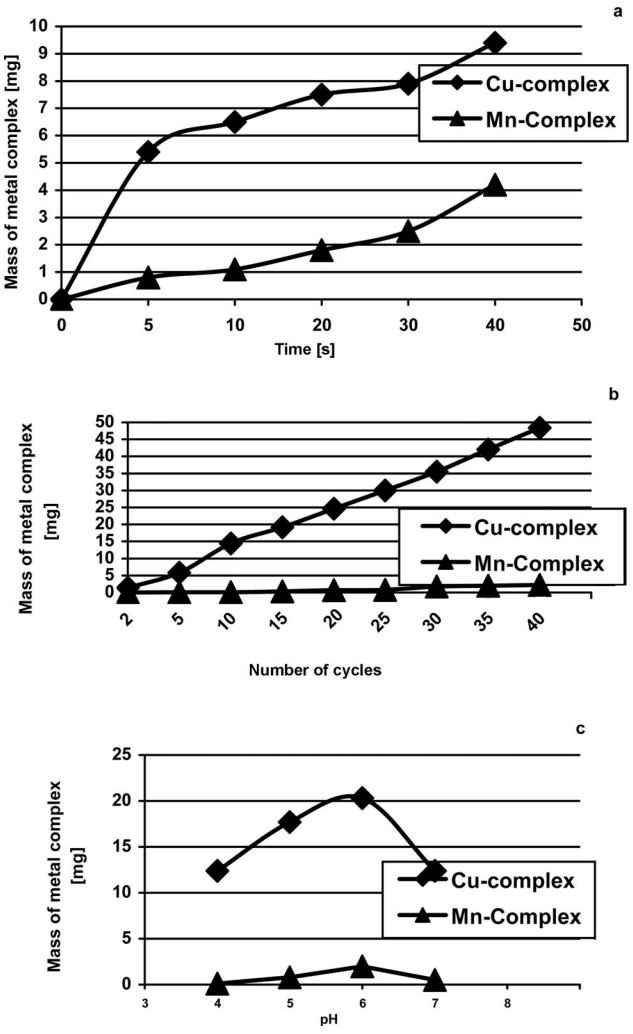

Figure 1. (a) Effect of dipping time on the mass of the thin films of the Cu complex (6 cycles) and the Mn complex (15 cycles). (b) Effect of the number of dipping cycles on the mass of the thin films of the Cu complex (10 s) and the Mn complex (20 s). (c) Effect of pH of solutions on the mass of thin films of the Cu and Mn complexes with a dipping time of 10 s.

Stoichiometry of Metal Complexes On the Basis of Metal Analysis and EIMS

Fast chemical reactions were observed for the formation of thin films of all the metal complexes when the glass substrate was first dipped into the metal ion solution and then into the ligand solution [H_2mna]. Metal analysis of the characterized LBL thin-films of the nanosized Mn^{II}, Co^{II}, Ni^{II}, Cu^{II}, and Zn^{II} complexes indicated that their reactions with [H_2mna] were similar. All newly synthesized nanosized $M[Hmna]_2$ complexes were found to exhibit a 1:2 molar stoichiometric ratio. This conclusion is based on the determination of the percentage of metal species in each complex, as listed in Table 2.

The electron impact mass spectra (EI-MS) can also be examined in order to confirm the molecular formula of the newly synthesized nanosized $M[Hmna]_2$ complexes. In the process of EIMS by direct insertion probe, the tested sample must be thermally stable with low melting point (<350 °C) in order to transfer to the ion source. Therefore, the complex $Mn[Hmna]_2$ was only subjected to EIMS analysis owing to it having the lowest melting of all the metal complexes listed in Table 2. The EIMS of the ligand [H_2mna] was also acquired for simple comparison with that of $Mn[Hmna]_2$. The EIMS of [H_2mna] was found to exhibit a characteristic molecular ion peak at m/z = 155 amu as the base peak. Several other characteristic fragment ion peaks are evident in the EIMS of [H_2mna] at m/z = 137, 111, 83, and 67 with relative intensity values of 35, 69, 26, and 72%, respectively. The two fragment ion peaks at m/z = 137 and 111 are related to the losses of H_2O and CO_2 from the molecular ion. The two peaks at m/z = 83 and 67 mainly arise from the fragment ions $[CHCHCCOOH]^{+\cdot}$ and $[CHCHCCOH]^{+}$, respectively. The EIMS of $Mn[Hmna]_2$ was found to exhibit the molecular ion peak at m/z = 363 amu with a relative intensity of 2.0%. Another fragment ion peak was identified at m/z = 209 (I_{rel} = 10%) and is related to the loss of the deprotonated ligand portion [Hmna] from the molecular ion. A fragment ion peak at m/z = 155 (I_{rel} = 97%) was also characterized in the EIMS of $Mn[Hmna]_2$ along with other fragment ions at 137 (I_{rel} = 32%), 111 (I_{rel} = 15%), 83 (I_{rel} = 51%), 67 (I_{rel} = 14%), and 55 (I_{rel} = 100%).

The collected data from the EIMS of the complex $Mn[Hmna]_2$ directly shows that the assigned structure of this complex has a 1:2 stoichiometric ratio. However, the other newly synthesized nanosized $M[Hmna]_2$ complexes

Table 2. Some characteristic data of nanosized $M[Hmna]_2$ complexes.[a]

Complex	Color	M.p. [°C]	$M_{theor.}$ [%]	$M_{exp.}$ [%]	No. dipping cycles
$Mn[Hmna]_2$	orange	320–325	Mn: 15.04	Mn: 14.77	35
$Co[Hmna]_2$	brown	>350	Co: 15.95	Co: 16.03	25
$Ni[Hmna]_2$	yellowish green	>350	Ni: 15.90	Ni: 15.91	25
$Cu[Hmna]_2$	black	>350	Cu: 17.00	Cu: 17.08	10
$Zn[Hmna]_2$	white	>350	Zn: 17.40	Zn: 17.47	40

[a] The listed data are based on sample particles collected from the deposited metal complex thin films.

are highly stable to the EIMS ionization conditions, as can be seen from their high melting point values given in Table 2.

SEM Analysis and Imaging of Nanosized M[Hmna]$_2$ Complexes

Figure 2 shows the SEM image of the deposited thin film of 2-mercaptonicotinic acid ([H_2mna]) on a glass substrate. This image was acquired for simple comparison with other thin films of the complexes M[Hmna]$_2$. The SEM images of the various metal complexes were found to be completely different from that of [H_2mna]. Figure 3shows the SEM images of the thin film of the complex Mn[Hmna]$_2$ deposited on a glass substrate after 35 cycles of alternate dipping in the metal ion solution followed by in the ligand ion solution. It was noticed that a fast complex reaction was found to proceed for the thin-film formation. Initially, for the Mn[Hmna]$_2$ complex, uniform complex particles were formed after a few dipping cycles. Figure 3(top) shows an SEM image of the deposited thin film of the complex Mn[Hmna]$_2$ at 5000× magnification and shows the high homogeneity and similarity in Mn[Hmna]$_2$ crystal growth based on LBL complex formation. The Mn[Hmna]$_2$ crystals shown in Figure 3(bottom) shows a simple aggregation of nanoparticles with the size 27–81 nm.

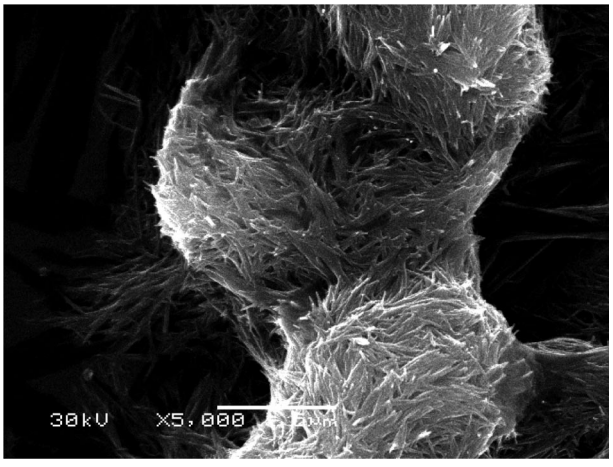

Figure 2. SEM image of the deposited thin film of 2-mercatonicotinic acid.

Figure 4 shows the SEM image (40000× magnification) of the thin film of the complex Co[Hmna]$_2$ deposited after 25 dipping cycles. Most of the particle sizes of Co[Hmna]$_2$ were identified to be in the range 25–41 nm. A fast complex formation reaction of the Co[Hmna]$_2$ thin films was also characterized after a few dipping cycles, in a fashion similar to the thin-film formation of Mn[Hmna]$_2$. Figure 5 presents an SEM image of a LBL deposited thin film of Ni[Hmna]$_2$, which shows a homogeneous particle distribution of Ni[Hmna]$_2$. The particle size was characterized to be in the range 8–24 nm, as determined from the SEM at 120000× magnification. Figure 6 shows an SEM image (40000× magnification) of the complex Cu[Hmna]$_2$ with an

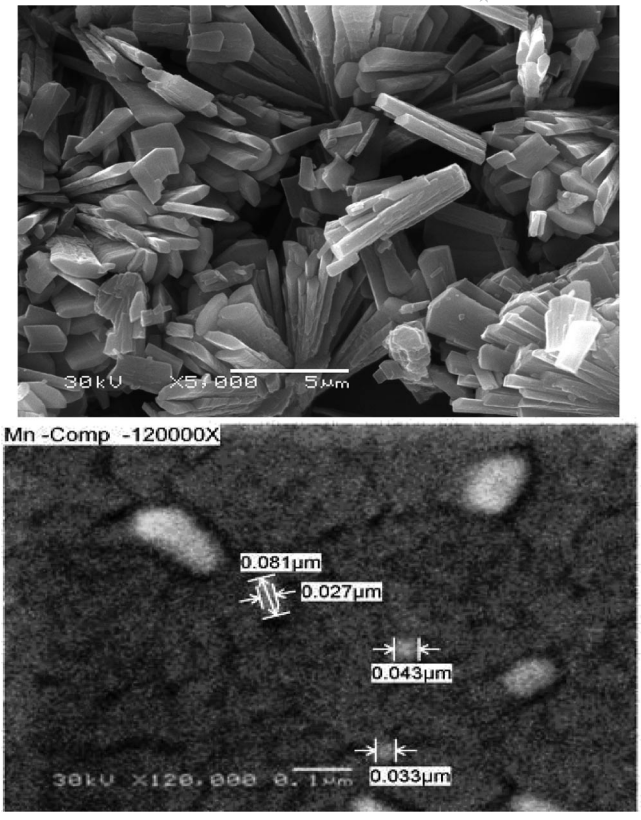

Figure 3. (i) SEM image of the thin film of the complex Mn[Hmna]$_2$ with a 5000× magnification, after 25 dipping cycles, and with a dipping time of 20 s. (ii) SEM image of the thin film of the complex Mn[Hmna]$_2$ with a 120000× magnification.

aggregate composition synthesized after only 10 dipping cycles by using the LBL deposition technique. The particle size distribution of the complexes Cu[Hmna]$_2$ was found to be in the range 53–139 nm. The homogeneity of the deposited nanoparticles of Cu[Hmna]$_2$ was studied by SEM imaging of the cross section of the thin film. Figure 7 gives a presentation of this image and provides evidence that the average film thickness is ≈1.982 μm, on the basis of six successive deposition cycles. Thus, one can easily identify that the thickness of one layer deposition per cycle is ≈330 nm, thus representing a deposited multimolecular Cu[Hmna]$_2$ complex. The SEM images of the deposited thin film of the complex Zn[Hmna]$_2$ after 40 dipping cycles is shown in Figure 8. The shape of Zn[Hmna]$_2$ is most likely a result of its anisotropic character. The detected particle size of the complex Zn[Hmna]$_2$ was found to be in the range 5–11 nm.

It is evident from the SEM study that all the synthesized metal–2-mercaptonicotinate complexes were found to grow from just a single molecule to several molecules in an aggregate distribution with particle size starting from few nanometers. In addition, various characteristic shapes of the metal complexes were also identified, and these SEM images are quite different from that of 2-mercaptonicotinic acid, which gives additional evidence for the formation of thin films of the nanosized metal complexes by the applied LBL technique.

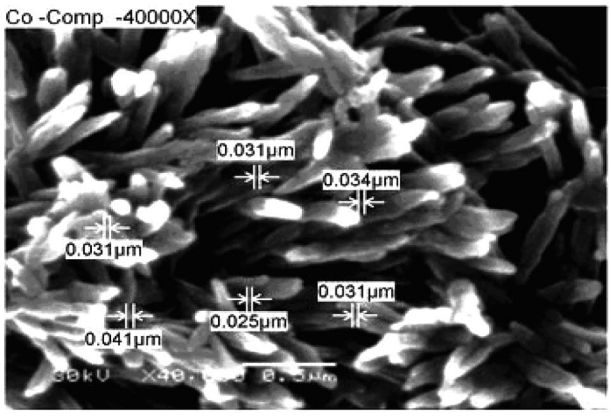

Figure 4. SEM image of the thin film of the complex Co[Hmna]$_2$ with a 40000× magnification, after 25 dipping cycles, and with a dipping time of 20 s.

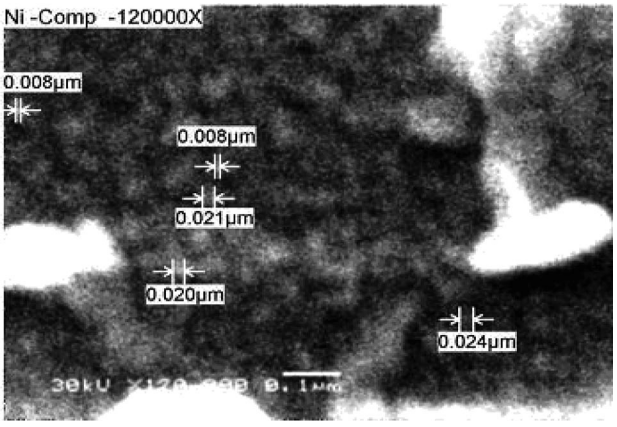

Figure 5. SEM image of the thin film of the complex Ni[Hmna]$_2$ with a 120000× magnification, after 25 dipping cycles, and with a dipping time of 20 s.

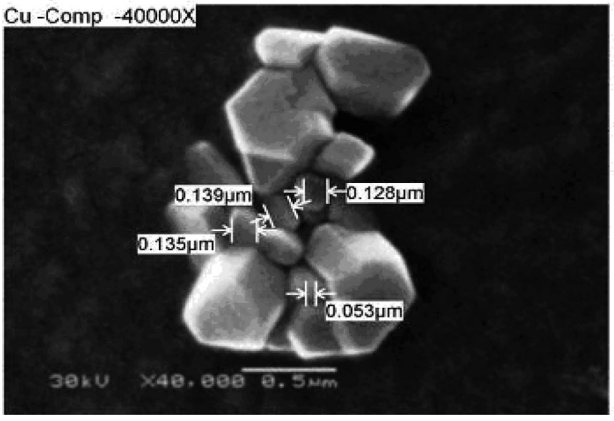

Figure 6. SEM image of the thin film of the complex Cu[Hmna]$_2$ with a 40000× magnification, after 10 dipping cycles, and with a dipping time of 20 s.

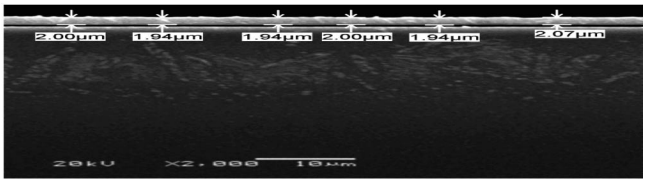

Figure 7. SEM image of a homogeneous thin-film cross section of Cu[Hmna]$_2$.

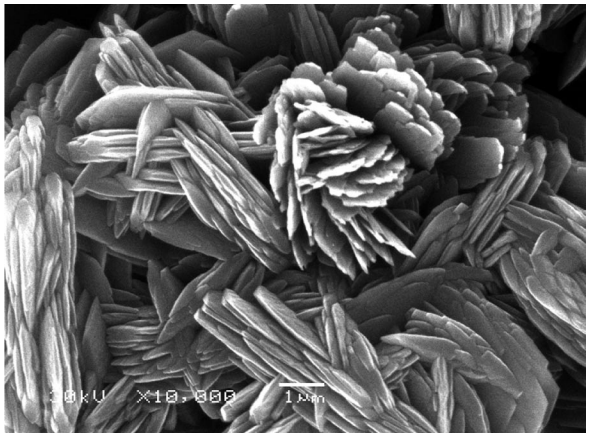

Figure 8. SEM image of the thin film of the complex Zn[Hmna]$_2$ with a 10000× magnification, after 40 dipping cycles, and with a dipping time of 20 s.

FTIR and UV/Vis of the Thin Films of M[Hmna]$_2$ Deposited by the LBL Technique

The FTIR spectrum of [H_2mna] was found to exhibit several characteristic absorption peaks that are related to the functional groups of the ligand. The absorption peaks located at 3496, 2409, and 1678 cm^{-1} are mainly assigned to the ν_{NH}, ν_{SH}, and ν_{COOH} stretching frequencies, respectively. The FTIR spectra of all newly synthesized nanosized, thin-film metal complexes were also characterized. In the FTIR spectra of the five thin-film complexes, the absorption peak for ν_{SH} was found to disappear owing to a deprotonation process. The FTIR spectra of the M[Hmna]$_2$ complexes show distinct vibrational bands at 1574–1597 and 1352–1383 cm^{-1}, assigned to ν_{CN} vibrations,[33] as well as at 1055–1078 and 628–650, attributed to ν_{CS} vibrations. The FTIR spectra of the free ligand shows characteristic peaks at 1568–1323 and 1056–634 cm^{-1}, assigned to ν_{CN} and ν_{CS} bands, respectively.[33] The most significant contribution was observed in the case of the ν_{CS} stretching frequency, which supports electron donation from the sulfur atom upon coordination to the metal ions. The peak assigned to the carboxyl group in the ligand moiety at 1678 cm^{-1} was found to disappear in all the FTIR spectra of the complexes M[Hmna]$_2$, which indicates the participation of the carboxylic group in the coordination process with the various metal ions.[33] Therefore, the FTIR studies reveal the possible coordination of the metal ions to the monoanionic [Hmna]$^-$ ligand through the S and O atoms. Figure 9 shows the FTIR spectrum of the complex Co[Hmna]$_2$ deposited on a substrate.

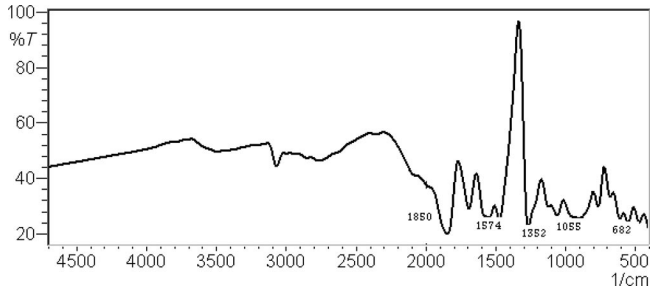

Figure 9. FTIR spectrum of the nanosized $Co[Hmna]_2$ complex deposited on the glass substrate.

The UV/Vis electronic spectra of the LBL deposited thin films of the complexes of $M[Hmna]_2$exhibit characteristic d–d transitions bands. This band is centered at ≈300 nm and at ≈380 nm for the $Mn[Hmna]_2$ complex (a broad band). The spectrum for the $Co[Hmna]_2$ complex shows a shoulder at ≈300 nm and a very weak band at ≈380 nm, and that of the $Ni[Hmna]_2$ complex exhibit a strong band at ≈300 nm and a shoulder at ≈380 nm. The spectrum for the $Cu[Hmna]_2$ complex shows a shoulder band at ≈380 nm. Figure 10 shows representative UV/Vis spectra for all $M[Hmna]_2$ complexes dissolved in methanol. Figure 11 presents the UV/Vis electronic spectrum of the complex $Co[Hmna]_2$ deposited on a substrate.

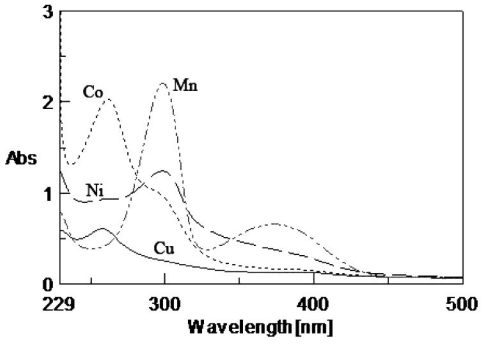

Figure 10. UV/Vis spectra of nanosized $M[Hmna]_2$ complexes in methanol.

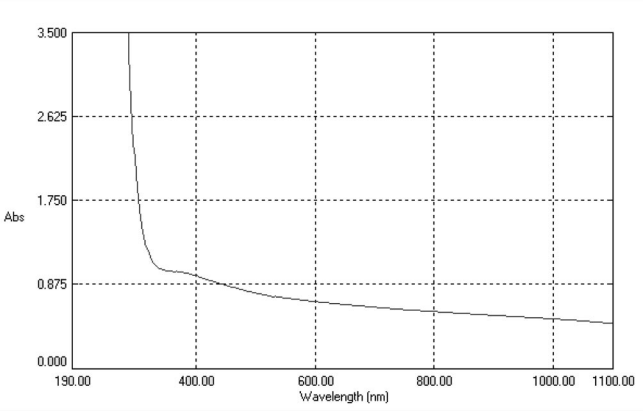

Figure 11. UV/Vis spectrum of the nanosized $Co[Hmna]_2$ complex deposited on the glass substrate after 25 dipping cycles and with a dipping time of 20 s.

Thermal Gravimetric Analysis of the Complexes $M[Hmna]_2$

Thermal gravimetric analysis of the LBL-synthesized $M[Hmna]_2$ complexes was also performed. The decomposition stages, temperature range, decomposition product, as well as the found and calculated percent mass losses are listed in Table 3. Several identified thermal degradation steps are mainly due to the direct decomposition of $[Hmna]^-$ in the metal complexes. The complexes $Co[Hmna]_2$ and $Cu[Hmna]_2$ show three possible degradation steps, with the identified metal oxides as the final stable products at ≥813 K. The TGA thermogram of $Mn[Hmna]_2$ shows only two degradation steps. The first step is related to the direct decomposition of a bound $[Hmna]^-$ molecule, followed by the second decomposition step of the

Table 3. Thermal behavior of the complexes $M[Hmna]_2$.

Complex (F_W)	T of DTG peak [K]	Temperature range [°C]	Decomposition product lost (F_W)	Mass found [%] (Mass calcd. [%])
$Mn[C_6H_4NO_2S]_2$ (362.9)	673	297–434	$C_6H_4NO_2S$ (138)	37.72 (38.02)
	793	434–599	$C_6H_4NO_2S$ (138)	36.54 (38.02)
			Residue MnO_2 (86.9)	25.73 (23.90)
$Co[C_6H_4NO_2S]_2$ (366.9)	159	44–267	½CO_2 (22)	5.06 (5.90)
	653	267–478	½CO_2 (22) + [$(C_5H_4N)_2$ + S] (210)	58.70 (57.23)
	813	478–599	[CO (28) + ¼S (8)] (36)	10.44 (9.81)
			Residue CoO_2 (90.9)	25.80 (24.78)
$Ni[C_6H_4NO_2S]_2$ (366.7)	373	24–266	2CO (56)	16.31 (15.27)
	653	266–397	(C_4H_3 + ½NH) (58.5)	15.19 (15.90)
	793	397–597	(1½NH + C_5H_4NS + O) (148.5)	40.15 (40.49)
			Residue ($NiO_2S_{1/2}$) (106.7)	28.35 (29.09)
$Cu[C_6H_4NO_2S]_2$ (371.55)	363	22–237	½CO (14)	4.10 (3.76)
	553	237–333	[½CO + $(C_5H_4N)_2$ + 1¾S] (226)	61.82 (60.83)
	813	495–598	(¼S + CO) (36)	9.84 (9.68)
			Residue CuO_2 (95.55)	24.611 (25.71)
$Zn[C_6H_4NO_2S]_2$ (373.39)	373	21–297	CO (28)	7.93 (7.50)
	673	297–468	(C_5H_4N + C_5H_4 + ½NH) (149.5)	39.79 (40.03)
	853	468–598	(½S + CO + ½NH) (51.50)	13.91(13.79)
			Residue ($ZnO_2S_{3/2}$) (145.4)	38.37 (38.94)

Table 4. Thermodynamic parameters of the $M[Hmna]_2$ complexes formed by LBL deposition.

Complex	Step	T [K]	n (reaction order)	Ln A	E_a [J mol^{-1}]	ΔH^* [kJ mol^{-1}]	ΔS^* [kJ mol^{-1} K^{-1}]	ΔG^* [kJ mol^{-1}]	r
$Mn[C_6H_4NO_2S]_2$	1	673	0.67	17.89	107.25	–5.049	–0.102	63.79	0.98082
	2	793	2	18.98	131.86	–6.46	–0.095	69.06	0.86139
$Co[C_6H_4NO_2S]_2$	1	159	1	7.65	27.84	–1.29	–0.176	26.83	0.96902
	2	653	1	7.69	52.25	–5.38	–0.187	117.01	0.93648
	3	813	1	11.68	86.38	–6.67	–0.156	120.27	0.91869
$Ni[C_6H_4NO_2S]_2$	1	373	1	7.33	26.52	–3.07	–0.185	66.25	0.87293
	2	653	1	16.09	90.71	–5.35	–0.117	71.59	0.98336
	3	793	1	9.18	69.34	–6.52	–0.176	133.52	0.97108
$Cu[C_6H_4NO_2S]_2$	1	363	2	6.05	17.6	–3.00	–0.196	68.22	0.51768
	2	553	2	25.34	117.47	–4.48	–0.039	17.28	0.70498
	3	813	1	17.34	127.45	–6.63	–0.109	82.05	0.97672
$Zn[C_6H_4NO_2S]_2$	1	373	2	8.84	27.26	–3.07	–0.173	61.55	0.82376
	2	673	2	20.97	120.55	–5.47	–0.077	46.57	0.951314
	3	853	0.67	15.94	119.72	–6.97	–0.121	96.34	0.97434

other $[Hmna]^-$ molecule, which gives rise to a residual component of MnO_2 at a temperature ≥793 K. The TGA thermograms of the complexes $Ni[Hmna]_2$ and $Zn[Hmna]_2$ show three degradation steps. These steps also correspond to the direct decomposition of a bound $[Hmna]^-$ molecule, which produces the corresponding $NiO_2S_{1/2}$ and $ZnO_2S_{3/2}$ products at temperatures ≥793 and ≥853 K, respectively.

The influence of the structural properties of the ligand and metal type on the thermal behavior of the complexes was evaluated. The order, n, the heat of activation, E_a*, of various decomposition stages were determined from the TGA and DTG thermograms by using the Borchardt and Daniels approach.[34] The identified kinetic parameters are listed in Table 4. The following points can be made. (i) The negative values of the activation entropy, ΔS^*, indicate a more ordered activated complex than the reactants, and/or the reactions are slow.[35] (ii) The activation enthalpy value, ΔH^*, increases from Mn^{II} to Zn^{II}, which corresponds to the gradual increase in stability of $M[Hmna]_2$ {M^{2+} (aq) + $2Hmna^-$ (aq) → $M[Hmna]_2$ (s)} (M = Mn, Co, Cu, Ni, and Zn). (iii) The values of the activation energy, ΔG^*, increase significantly according to the decomposition stages of a given complex. This mainly arises because of the increasing values of $T\Delta S^*$ from one step to another, which override the values of ΔH^*. The increasing values of ΔG^* for subsequent steps for a given complex reflects that the rate of removal of the subsequent ligand will be lower than that of the preceding ligand.[36,37] This may be attributed to the greater structural rigidity of the remaining complex after the expulsion of one and more ligands, relative to that of the preceding complex, which requires more energy. (iv) The reaction orders of the decomposition steps were found to be 0.67, 1, and 2. It should be emphasized that the reaction order of a solid-state decomposition has no intrinsic meaning, but it is rather a mathematical smoothing device (parameter).[38]

Conclusion

The research work presented here indicates a novel synthetic approach for thin-film growth and control of discrete nanometal complexes. In addition, the results outlined point to the suitability and generality of the LBL chemical deposition technique for thin-film formation of nanosized metal complexes through a simple, rapid, and efficient approach; the nanosized metal complexes were obtained at room temperature in a 1:2 stoichiometric ratio after only a few dipping reaction cycles and a few seconds of reaction. The particle size of the newly synthesized compounds was found to be in the range 20–130 nm. The advantages of the LBL chemical deposition technique are evident in terms of time and reaction conditions when compared to the bulk synthesis of these metal complexes.[28] In addition, synthesis of nanosized metal complexes in a thin-film assembly, as described in this work, can lead to further studies of thin-film evaluation in various disciplines. Accordingly, a study to characterize the potential applications of newly synthesized metal complexes as optically and/or electrically active nanomaterials is currently underway.

Experimental

Chemicals and Materials

The metal salts were purchased from Aldrich Chemical Company, USA, and BDH Limited, Poole, England, and were all of analytical grade. Metal acetate or chloride salts were used, cobalt acetate [$Co(OAC)_2{\cdot}4H_2O$], nickel acetate [$Ni(OAC)_2{\cdot}4H_2O$], copper acetate [$Cu(OAC)_2{\cdot}H_2O$], zinc acetate [$Zn(OAC)_2{\cdot}2H_2O$], and manganese chloride [$MnCl_2{\cdot}4H_2O$]. 2-Mercaptonicotinic acid (H_2mna) and ethanol were obtained from BDH Limited, Poole, England, and used as received. The metal ion solutions (0.1 M) were prepared with doubly distilled water by dissolving the appropriate mass of the metal salt in a 500-mL flask. A 0.2 M ethanol solution of (H_2mna) was also prepared and used. The microslide glass substrates (76.2, 25.4, and 1.0 mm) were cleaned as previously reported.[12]

Layer-by-Layer Thin-Film Formation of the Metal Complexes

General Procedure: The formation of the complexes $M[Hmna]_2$ [M = Mn^{II}, Co^{II}, Ni^{II}, Cu^{II}, and Zn^{II}] was performed by chemical dipping according to the following procedure. The synthetic approach for the synthesis of nanosized metal complexes was based

on thin-film formation by LBL deposition. A solution of metal acetate or chloride (0.1 M) was prepared with doubly distilled water. A solution of 2-mercaptonicotinic acid (0.2 M) was prepared and dissolved in absolute ethanol with the addition of few drops of NaOH (0.2 M). A clean glass substrate was vertically immersed into the metal ion solution for a 20-s period to deposit the corresponding metal ion onto the surface of the substrate (first step). The substrate was then immersed in the ligand solution for another 20 s, where as the predeposited metal ion on the glass substrate was allowed to react with the ligand (second step). These two deposition reaction steps generally represents the dipping cycle. A colored and uniform thin film of the metal complex was formed after a few dipping cycles. The reaction substrate was rinsed with distilled water after each reaction cycle. This procedure was repeated several times [10–40 times] to increase the film thickness and homogeneity. In addition, the metal complexes were prepared in the absence of water by rinsing between successive cycles.

Studied and Optimized Factors: The influence of the number of dipping cycles on the formation of thin films of the complexes $Mn[Hmna]_2$ and $Cu[Hmna]_2$ was studied at constant immersion time, 20 and 10 s, respectively. The selected number of dipping cycles for this study was (2, 5, 10, 20, 30, and 40) and (10, 15, 20, 25, and 30), respectively. The influence of the immersion time on the formation of thin films of the complexes $Mn[Hmna]_2$ and $Cu[Hmna]_2$ was also studied. The times used were 5, 10, 20, 30, and 40 s, with a 1:2 metal to ligand stoichiometric ratio and 6 $\{Cu[Hmna]_2\}$and 15 $\{Mn[Hmna]_2\}$ dipping cycles. The influence of the pH of the metal ion and ligand solution on the formation of thin films of the complexes $Mn[Hmna]_2$ and $Cu[Hmna]_2$ was also studied for metal ion solutions with pH 4, 5, 6, and 7, with a 1:2 metal to ligand stoichiometric ratio, an immersion time of 10 s, and 10 dipping cycles.

Instrumentations: A scanning electron microscope (JSM-6360 LA, JEOL Ltd.), (JSM-5300, JEOL Ltd.), and an ion sputtering coating device (JEOL-JFC-1100E) were used to examine and image the deposited thin films of the metal–2-mercaptonicotinate complexes. SEM specimens were coated with gold to increase the conductivity. The FTIR spectra of 2-mercaptonicotinic acid and the complexes $M[Hmna]_2$ were measured on a Shimadzu Fourier Transform infrared spectrophotometer (FT-IR-8400S) in the range 4000–200 cm^{-1}. The thermal gravimetric analysis (TGA) and thermoanalytical curves were obtained by using a Perkin–Elmer TG A7 Thermobalance. The operating conditions were as follows: a temperature heating range of 20–600 °C with heating rate of 10 °C min^{-1}, a flow rate of 20 mL min^{-1} in a pure nitrogen atmosphere, and a sample mass in the range (5.0–7.0 mg). Shimadzu gas chromatography mass spectrometer (GC–MS-QP2010 plus) equipped with a direct insertion probe (DIP), microanalytical laboratory-Cairo University, was used to acquire the electron impact mass spectra (EIMS) of 2-mercaptonicotinic acid and its $Mn[Hmna]_2$ complex with 70 eV as the ionization energy. Heating temperature programming of the DIP was performed at 50 °C min^{-1}. The maximum temperature was adjusted to 350 °C, and the run time was completed in 8.0 min. UV/Vis spectra of the metal–2-mercaptonicotinate complexes were measured on a Perkin–Elmer UV/Vis spectrometer Lambda EZ 210. Metal analysis of the 2-mercaptonicotinate complexes was determined on a Shimadzu (AA-6650) atomic absorption spectrophotometer after acid decomposition and suitable dilution.

Acknowledgments

I am deeply grateful to Professor Dr. Mohamed E. Mahmoud, Chemistry Department, Faculty of Sciences, Alexandria University, Egypt for his valuable guidance and technical support during the course of this work.

[1] C. W. Lee, J. G. Kim, M. S. Young, *Macromol. Res.* **2005**, *13*, 265–273.
[2] K. Ariga, J. P. Hill, Q. Ji, *Phys. Chem. Chem. Phys.* **2007**, *9*, 2319–2340.
[3] Y. Wang, A. S. Angelatos, F. Caruso, *Chem. Mater.* **2008**, *20*, 848–858.
[4] D. Wakizaka, T. Fushimi, H. Ohkita, S. Ito, *Polymer* **2004**, *45*, 8561–8565.
[5] F. Caruso, X. Shi, R. A. Caruso, A. Susha, *Adv. Mater.* **2001**, *13*, 740–744.
[6] N. Laugel, J. Hemmerlé, C. Porcel, J. Voegel, P. Schaaf, V. Ball, *Langmuir* **2007**, *23*, 3706–3711.
[7] N. Laugel, J. Hemmerlé, N. Ladhari, Y. Arntz, E. Gonthier, Y. Haikel, J. Voegel, P. Schaaf, V. Ball, *J. Colloid Interface Sci.* **2008**, *324*, 127–133.
[8] T. Fushimi, A. Oda, H. Ohkita, S. Ito, *J. Phys. Chem.* **2004**, *B108*, 18897–18902.
[9] T. Fushimi, A. Oda, H. Ohkita, S. Ito, *Langmuir* **2005**, *21*, 1584–1589.
[10] T. Fushimi, A. Oda, H. Ohkita, S. Ito, *Thin Solid Films* **2005**, *484*, 318–323.
[11] H. Benten, N. Kudo, H. Ohkita, S. Ito, *Thin Solid Films* **2009**, *517*, 2016–2022.
[12] M. E. Mahmoud, S. S. Haggag, T. M. Abdel-Fattah, *Polyhedron* **2009**, *28*, 181–187.
[13] M. E. Mahmoud, S. S. Haggag, M. Abdel Rafea, T. M. Abdel-Fattah, *Polyhedron* **2009**, *28*, 3407–3414.
[14] T. Itoh, T. Schichi, T. Yui, H. Takahashi, Y. Inui, K. Takagi, *J. Phys. Chem. B* **2005**, *109*, 3199–3206.
[15] C. Wang, Z. Ma, *Anal. Bioanal. Chem.* **2005**, *382*, 1708–1710.
[16] J. Kim, J. M. Kim, D. J. Ahn, *Macromol. Res.* **2006**, *14*, 478–482.
[17] Y. Aoki, T. Kunitake, A. Nakao, *Chem. Mater.* **2005**, *17*, 450–458.
[18] G. Freiman, P. Barboux, J. Perriere, K. Giannakopoulos, *Thin Solid Films* **2009**, *517*, 2670–2674.
[19] X. L. Zheng, J. B. Weng, Q. M. Huang, B. H. Hu, T. Qiao, P. Deng, *Colloids Surf. Physicochem. Eng. Aspects* **2009**, *337*, 15–20.
[20] T. G. Shutava, S. S. Balkundi, Y. M. Lvov, *J. Colloid Interface Sci.* **2009**, *330*, 276–283.
[21] T. M. Benedetti, F. F. C. Bazito, E. A. Ponzio, R. M. Torresi, *Langmuir* **2008**, *24*, 3602–3610.
[22] T. Berzina, L. Cristofolini, V. Erokhin, C. Folli, M. P. Fontana, *Langmuir* **2008**, *24*, 12093–12096.
[23] H. M. Pathan, C. D. Lokhande, *Bull. Mater. Sci.* **2004**, *27*, 85–111.
[24] M. E. Mahmoud, *J. Liq. Chrom. Relat. Technol.* **2002**, *25*, 1187–1199.
[25] J. F. Read, C. R. Graves, E. Jackson, *Inorg. Chim. Acta* **2003**, *348*, 41–49.
[26] L. Zhang, H. Zhang, C. Chen, L. Deng, B. Kang, *Inorg. Chim. Acta* **2003**, *355*, 49–56.
[27] S. P. Chen, Q. Yang, S. Gao, *J. Therm. Anal. Calor.* **2009**, *95*, 685–689.
[28] Q. Yang, S. Chen, S. Gao, *J. Therm. Anal. Calor.* **2007**, *90*, 881–885.
[29] G. Rabbani, A. A. Isab, A. R. Al-Arfaj, S. Amad, M. Saleem, A. Hameed, E. Akbar, *Spectroscopy* **2009**, *23*, 45–50.
[30] S. Marchal, V. Moreno, G. Aullon, S. Alvarez, M. Quiros, M. Font-Bardia, X. Solans, *Polyhedron* **1999**, *18*, 3675–3682.
[31] F. N. Rein, H. E. Toma, *Polyhedron* **1998**, *17*, 1439–1448.
[32] S. M. O. Quintal, H. I. S. Nogueira, V. Félix, M. G. B. Drew, *J. Chem. Soc., Dalton Trans.* **2002**, 4479–4487.
[33] K. Nakamoto, *Infrared Spectra of Inorganic and Coordination compounds*, Wiley, New York, **1997**.

[34] H. J. Borchardt, F. J. Daniels, *J. Am. Chem. Soc.* **1957**, *79*, 41–46.
[35] A. A. Frost, R. G. Pearson, *Kinetics and Mechanisms*, Wiley, New York, **1961**.
[36] P. B. Marawalli, T. R. Goudar, *Thermochim. Acta* **1999**, *325*, 35–41.
[37] K. K. M. Yusuff, R. Sreekala, *Thermochim. Acta* **1990**, *159*, 357–368.
[38] D. B. Brown, E. G. Walton, *J. Chem. Soc., Dalton Trans.* **1980**, 845–850.

Received: December 2, 2009
Published Online: February 23, 2010

